16-Ch Time-resolved Single-Molecule Spectroscopy Using Line Excitation

Antonino Ingargiola[a*], Pietro Peronio[b], Eitan Lerner[a], Angelo Gulinatti[b], Ivan Rech[b], Massimo Ghioni[b], Shimon Weiss[a], Xavier Michalet[a+]

[a]Dept. Chemistry & Biochemistry, University of California Los Angeles, Los Angeles, CA, USA
[b]DEIB, Politecnico di Milano, Milan, Italy.

Abstract: Single-molecule spectroscopy on freely-diffusing molecules allows detecting conformational changes of biomolecules without perturbation from surface immobilization. Resolving fluorescence lifetimes increases the sensitivity in detecting conformational changes and overcomes artifacts common in intensity-based measurements. Common to all freely-diffusing techniques, however, are the long acquisition times.

We report a time-resolved multispot system employing a 16-channel SPAD array and TCSPC electronics, which overcomes the throughput issue. Excitation is obtained by shaping a 532 nm pulsed laser into a line, matching the linear SPAD array geometry. We show that the line-excitation is a robust and cost-effective approach to implement multispot systems based on linear detector arrays.

Keywords: single-molecule, fluorescence, high-throughput, TCSPC, SPAD array.

* ingargiola.antonino@gmail.com
+ michalet@chem.ucla.edu

1 Introduction

Fluorescence-based single-molecule techniques allow identifying sub-populations, detecting conformational changes or binding-unbinding events of single biomolecules in a heterogeneous sample.[1] Experiments on surface-immobilized molecules can be affected by the steric or chemical interference of the binding surface.[2] By contrast, experiments on unbound or freely-diffusing molecules are free from such perturbations. In such measurements, resolving lifetimes increases the ability to detect conformational changes and overcomes artifacts common in intensity-based measurements.[3–8] Freely diffusing single-molecule techniques traditionally employ a single diffraction limited spot to excite the sample. At suitable single-molecule concentrations of 100 pM or less, at most one molecule diffuses through the excitation spot at any given time. In practice, the concentration is adjusted such that the probability of having two molecules crossing the excitation spot at the same time can be considered negligible. Under these conditions, most of the time, no molecule is present in the excitation spot, which results in long acquisition times ($\sim 5 - 10$ min.) in order to accumulate enough single-molecule "events" (i.e. diffusions through the excitation spot resulting in a burst of photons).

To overcome this limitation, we recently introduced a multispot excitation/detection scheme that allows performing high-throughput single-molecule FRET (smFRET) experiments by parallelizing data acquisition.[9,10] This development was made possible by new SPAD arrays fabricated with a custom silicon technology with performance compatible with single-molecule detection.[11] The multispot excitation consists of an array of excitation spots generated using a liquid-crystal on silicon (LCOS) spatial light modulator (SLM) illuminated with a high power laser, the geometry of the excitation pattern matching the geometry of the SPAD arrays. While flexible, this approach requires high-performance and costly LCOS-SLMs and a careful optical design and alignment.

Single Molecule Spectroscopy and Superresolution Imaging X, edited by Jörg Enderlein, Ingo Gregor, Zygmunt Karol Gryczynski, Rainer Erdmann, Felix Koberling, Proc. of SPIE Vol. 10071, 100710Q · © 2017 SPIE · CCC code: 1605-7422/17/$18 · doi: 10.1117/12.2256367

Here we introduce a variant of this setup employing an alternative "line-excitation" scheme which only requires the addition of a single cylindrical lens to a standard confocal setup, dispensing altogether of the expensive LCOS-SLM. The line-excitation approach is a cost effective, and easy to implement solution for high-throughput single-molecule experiments and was previously used by the Takahashi group for intensity-based smFRET measurements of protein folding.[12,13] Their configuration involved a linear microfluidic channel in which single-molecule flowed through the line excitation and a electron-bombarded CCD camera for detection. Here, we use a simple standing drop, freely-diffusing single molecule sample and a 16-pixel SPAD array connected to a 16-channel TCSPC module,[14,15] demonstrating high-throughput lifetime-based smFRET measurements on simple model DNA molecules.

2 Materials and Methods

2.1 Setup Description

A schematic representation of the setup is shown in Fig. 1. The setup is based on a modified IX 71 inverted microscope (Olympus, Piscataway, NJ). As in a conventional confocal setup, a laser beam (LDH-P-FA-530XL, PicoQuant GmbH, Berlin, Germany; wavelength 532 nm, pulse width $<$100 ps, pulse repetition rate 20 MHz) is expanded in order to overfill the back aperture of the objective lens (Olympus UPlanApo 60x, N.A. 1.2 water). As shown in Fig. 1, the expanded laser beam passes through a 200 mm focal length cylindrical lens (LJ1653RM-A, Thorlabs Inc, NJ, USA) placed at a 200 mm distance from the back-aperture of the objective lens. The beam enters the microscope optical path through a dichroic mirror (*DM* in Fig. 1, dual edge 532-635nm) and is focused in one direction (y in Fig. 1) in the back-aperture of the objective lens. The objective lens generates the excitation line in the sample, and collects the fluorescence emission, which is then separated from the excitation beam by the dichroic mirror. The emitted light is further filtered with a band pass filter to reject laser reflection and Raman scattering and relayed to the bottom port of the microscope through the microscope tube lens. Additional relay optics consisting of 150 mm and 100 mm focal length doublet lenses (not shown) form the final image on the active area of a linear 32-pixel SPAD array,[15] 16 of which were used in this work due to the 16-channel capacity of the TCSPC electronics. Fig. 2 shows two orthogonal projection illustrating the principle used to generate the excitation line.

The SPAD array is characterized by dark count rates (DCR) varying from pixel to pixel, as reported in Fig. 4. The 16-channel TCSPC module is based on integrated time-to-amplitude converters (TAC) and has a mean resolution of 3.3 ps (minimum TCSPC bin size) and 2^{14} bins ($\sim$50 ns measurement window) . Due to the internal TAC architecture, the TCSPC resolution (i.e. bin size), varies slightly from channel to channel and needs to be calibrated (once) prior to performing experiments. The variation of the resolution across channel was found to be $<$6 % for the module used in these experiments.

Data processed and recorded by the TCSPC electronics consists of a stream of single-photon information, transferred via a USB-2 interface to the host computer. Each photon information comprises a channel number (0..15), a macrotime stamp (time since the beginning of the experiment, 50 ns resolution) and a nanotime stamp, or time until the next laser pulse (channel-dependent resolution, as discussed above), as classically provided by most TCSPC electronics.[16] This stream of photon is read asynchronously by a custom software written in LabVIEW, which displays intensity time traces, builds nanotime histograms for each channel, and saves data continuously to disk.

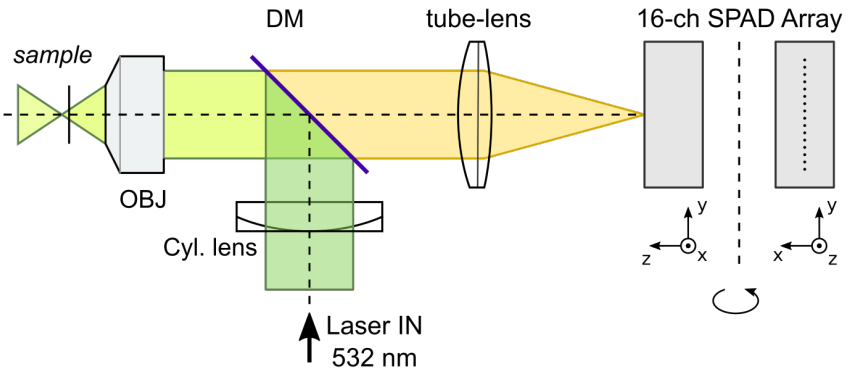

Fig 1 Schematic of the optical setup. An expanded laser beam is focused by a cylindrical lens on the back-aperture of the objective lens, generating an excitation line in the sample. The emission is detected by a 16-channel linear SPAD array placed on the image plane. See text for details.

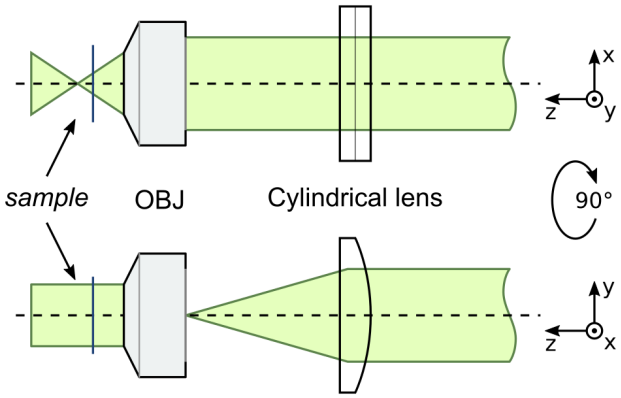

Fig 2 Scheme used to generate the excitation line as seen through two orthogonal projections. The cylindrical lens focuses the expanded laser beam on the back-aperture of the objective lens in one direction (y), while the other direction (x) is unaffected. The objective lens focuses the beam in the sample along the x direction while creating an expanded beam in the y direction.

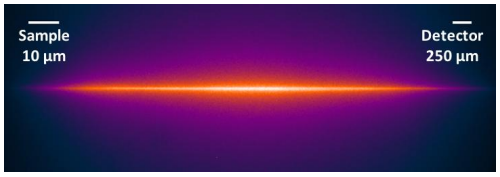

Fig 3 Experimental emission of an high-concentration dye solution (ATT0550) excited by the line pattern and recorded by a camera placed in the SPAD image plane.

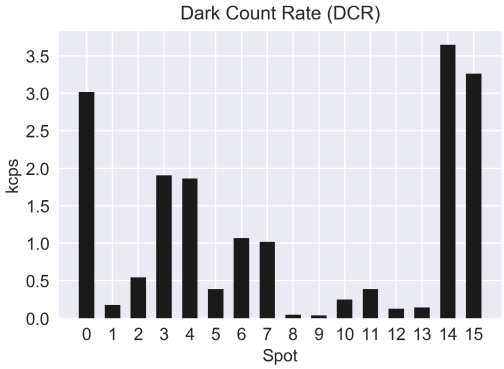

Fig 4 Dark-counting rates for the 16-pixel SPAD array used in this work.

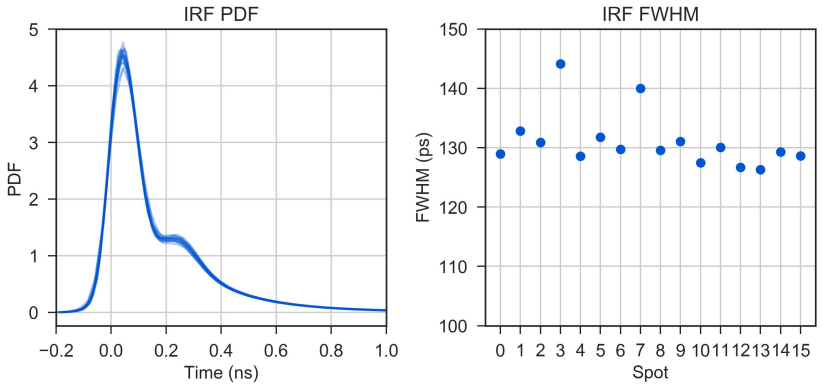

Fig 5 Experimental IRF for the 16 channels. Left plot: IRF histograms normalized to unit area (16 superimposed curves one for each channel). Right plot: IRF full-width at half maximum (FWHM) computed for each channel.

Fig. 5 shows experimental IRFs for the 16 channels, measured using the reflection from a cover-glass air interface. These IRFs include both laser and detection electronics contributions (SPAD + TCSPC hardware) and are characterized by FWHM of ∼130 ps for all but channels 3 and 7, having FWHM of 144 ps and 140 ps respectively.

2.2 Alignment

To facilitate the alignment, the SPAD array is placed on a 3-axis manual micro-positioner stage. The cylindrical lens is placed on a rotary holder (RSP1, Thorlabs). A sample with high concentration of ATTO50 dye (10-100 nM) generates a stable emission line used for alignment of the detector. For the alignment, a LabVIEW acquisition software displays intensity time traces of the 16 channels in real time. The rotation of the cylindrical lens, which directly sets the orientation of the line, is calibrated by translating the SPAD in a direction orthogonal to the excitation line while observing the time traces on the different channels. If the excitation line is perfectly parallel to the 16 pixels, all time traces will exhibit a signal maximum at the same time. Conversely, if there is an angle mismatch, time traces in different channels will exhibit maxima shifted in time. This visual feedback allows to iteratively adjust the orientation of the excitation line until convergence. Once the rotation angle is fixed, the SPAD array can be easily aligned in the X and Y directions in order

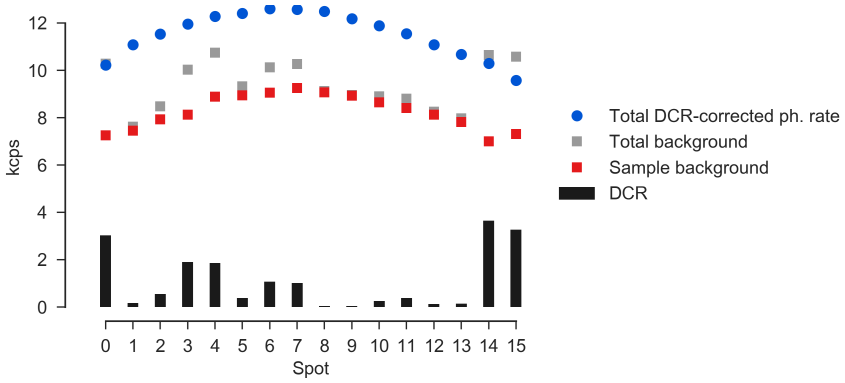

Fig 6 Various measurement statistics as function of spot. *(blue circles)* Total DCR-corrected photon rate; *(grey squares)* total background rate; *(red squares)* background from sample, i.e. total background rate minus DCR; *(black bars)* SPAD array's DCR.

to maximize the signal in all channels. This procedure results in the maximum uniformity of the signal across the 16 channels.

2.3 Measurements

To demonstrate the performance of the system, we report measurements of 80-base pair dsDNA samples, labeled with either a single ATTO550 label (ATTO-TEC GmbH, Heidelberg, Germany) or with two FRET labels (donor: ATTO550, acceptor: ATTO647N, ATTO-TEC) located 12 base-pairs apart. The DNA sequence is identical to that described in ref. 10 for real time transcription kinetic experiments (donor labeling on the non-template strand at position -3 and acceptor labeling in the template strand at position -15). Sample were diluted to single-molecule concentrations with TE50 buffer (10 mM Tris, 1 mM EDTA, bring to pH 8.0 with HCl, 50 mM NaCl). In order to acquire enough statistics in each individual spot, acquisition duration for single-molecule measurement range from 15 to 20 minutes. Data analysis is performed with the open source python software FRETBursts[17] and with the free LabVIEW software ALiX.[10] Jupyter notebooks used for the analysis are available on github (https://github.com/tritemio/polimi_tcspc_16ch). The measurement data files are stored in the open format Photon-HDF5[18] and are available on Figshare.[19]

3 Discussion and Results

3.1 Spot Characteristics

Fig. 6 shows total signal, background and DCR as function of the spot number. The total background rates (*gray squares*) are in the 8-10 kcps range and can be decomposed into sample background (*red squares*), due to buffer impurities, out-of-focus molecules fluorescence, etc., and DCR (*black bars*), measured separately in the absence of any signal. While DCR is responsible for most of the pixel-to-pixel fluctuations of the total background, the sample background is the dominant contribution for all but the noisiest pixels.

The DCR-corrected total signal, i.e. the total photon count rate minus DCR (Fig. 6, *blue circles*), exhibits a smooth convex profile. As expected, this corrected signal profile is similar to the intensity profile of the line-excitation pattern (see Fig. 3).

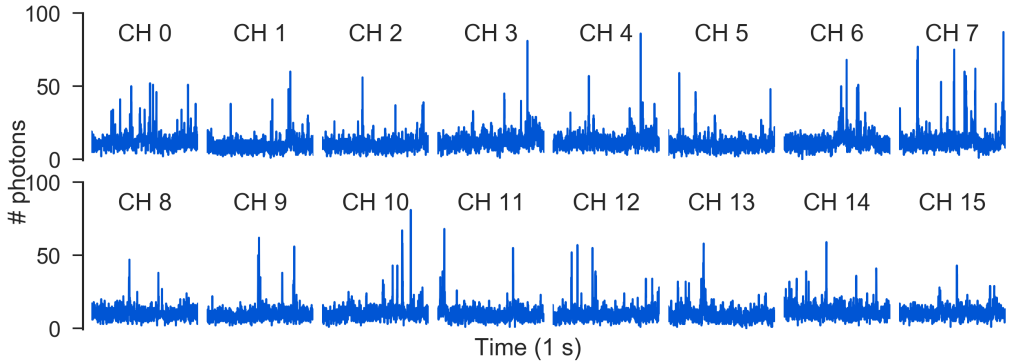

Fig 7 Timetraces (duration 1 s, bin size 1 ms) in 16 channels for a single-molecule measurement of a dsDNA sample labeled with ATTO550.

Fig. 7 represents typical time traces showing single-molecule bursts for all 16 channels (time trace duration 1 s, bin size 1 ms). Fig. 8 reports several burst statistics corresponding to two different burst search parameters sets. Using a burst search imposing a constant and identical count rate-threshold for burst start and stop in all spots[17] (*blue dots*), we note that the number of bursts and mean burst statistics (size, duration, peak photon rate) all follow a "peak" profile, similar to the profile of the total signal (Fig 6). However, the total signal of Fig. 6 exhibited a smaller relative variation between central and lateral pixels compared to any burst statistics.

Moreover, among the burst statistics of Fig. 8, the mean burst size (Panel B) exhibits more pronounced variations compared to burst duration (Panel C) and peak photon rate (Panel D). This can be understood by noticing that, to first order, the burst size can be approximated by the product of burst duration and peak photon rate. Finally, the "peak burst photon rate" (Fig. 8 *Panel D*) is a measure of the peak PSF intensity (including the product of excitation, emission and detection efficiencies). Assuming perfect alignment and uniform photon detection efficiency across the pixels, the peak burst photon rate is a measure of the peak excitation intensity at each pixel position.

To understand how the PSF profile (height and width) changes across the spots, we performed a second burst search with count rate-thresholds scaling with the mean "peak burst photon rate" (Fig. 8, *red squares*). Loosely speaking, this burst search sets a detection threshold equivalent to imposing that the molecule traverses the PSF at a location where its intensity is equal to a given fraction of its peak intensity. Therefore we call it for brevity *FWHM burst search*. First, we observe that the mean "peak burst photon rate" is unchanged compared to the previous burst search. This statistics is linearly dependent on the height of the PSF's peak (where the emission rate is maximum) and can be reasonably used to estimate changes in the PSF height. Second, the number of bursts obtained with FWHM burst search (*Panel A, red squares*) is now relatively constant across the spots. Third, the mean burst duration (*Panel C, red squares*) has an inverted trend: bursts on lateral pixels have larger mean duration than bursts on the central ones. These three observations can be rationalized as follows. As we move from the central spots to the lateral ones, the peak PSF intensity decreases as indicated by the trend in the mean "peak burst photon rate". At the same time, the PSF's width increases (larger burst duration), resulting in smaller but wider PSF. Finally, the mean burst size (*Panel B, red squares*) becomes only marginally smaller on the lateral spots, indicating that the larger PSFs width compensates (at least partially) for the loss in intensity. In other words, while moving from the central to the lateral spots, the PSF peak

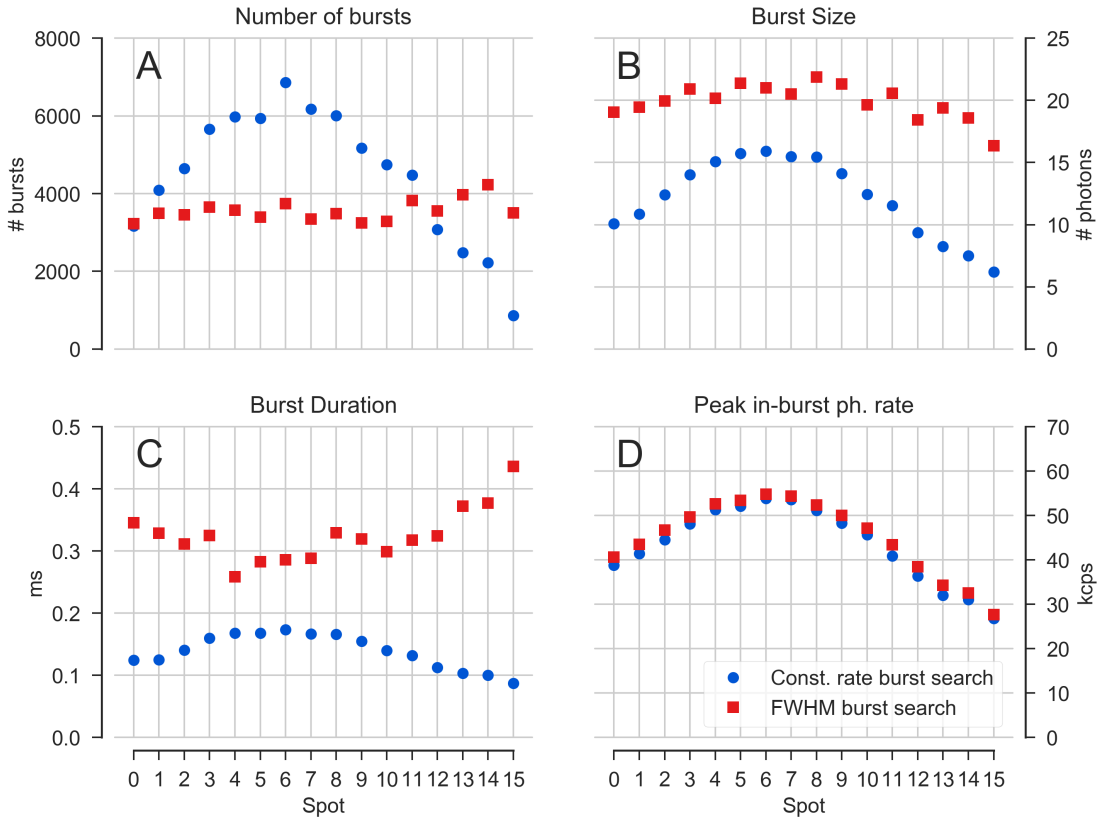

Fig 8 Burst statistics obtained with two burst searches: (*blue dots*) burst search using a constant rate-threshold (70 kcps) for all the spots; (*red squares*) burst search with a rate threshold scaling with the mean "peak burst photon rate" in each spot. *Panel A*: number of bursts after a size threshold of 20 photons. *Panel B*: mean burst size. *Panel C*: mean burst duration. *Panel D*: mean "peak in-burst photon rate".

decreases and its width increases, but its integral remains relatively constant.

3.2 Fluorescence Lifetime Results

Fig. 9 reports 16-channel lifetimes histograms normalized to unit area for the D-only sample. The histograms are computed from all bursts photon nanotimes, where bursts are defined as discussed in the previous section. To showcase the lifetimes-resolving capabilities of the setup, we performed two kind of analysis. In the first, we fitted the fluorescence decay (nanotime) histograms obtained from all burst photons to a sum of decaying exponentials convolved with the Instrument Response Function (IRF). In the second approach, used for the donor-only sample, we computed the mean lifetime for each burst and mean lifetime distribution for each channel as detailed later in the text.

In order to fit the fluorescence decays, we acquired IRF of each channel collecting the laser light reflected by a bare glass coverslip and building the nanotime histogram (Fig. 5). The fit of fluorescence decay histograms was performed by non-linear least squares minimization using the simplex downhill algorithm[20] as implemented in ALiX (https://sites.google.com/a/g.ucla.edu/alix/windows/nanotime-histogram-analysis). Uncertainty on each component's estimated lifetime are were computed as described in 21. In general, 2 or 3 components were used to obtain a satisfactory fit, due to the presence of some noticeable Raman or

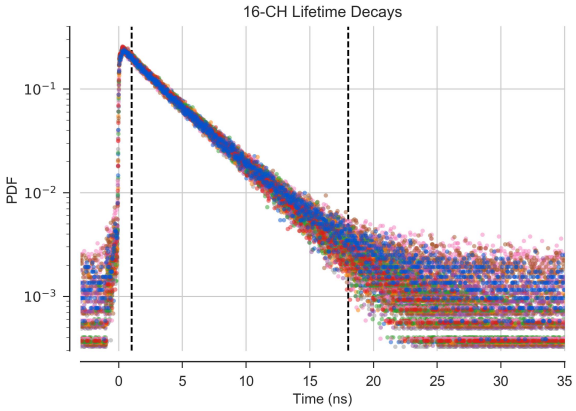

Fig 9 Normalized lifetime histograms for the 16 channels. For visualization, the original TCSPC nano-times are 8x binned, resulting in displayed bin size of ∼26.5 ps. The vertical dashed lines indicate the range of 1-18 ns used to compute per-burst mean lifetimes (see text for details).

Rayleigh scattering (as seen in Fig. 12) and the impossibility to separate donor-only bursts from FRET only bursts. The short component ($\leq$10 ps) represents a small fraction of the total counts in the decay, but is needed to account for the shape decay at short time scales. When two additional components were needed, one of them resulted in a lifetime close to that of the donor lifetime, consistent with the idea that detected bursts comprise a fraction of donor-only molecules.

Fig. 10 shows the fitted lifetimes values in the different channels for two samples (D-only and FRET). Fig. 12 shows the fitted fluorescence decays curves for two representative channels for both donor-only (D-only) and FRET sample. Except for channel 8, the main fitted lifetime values are within $\pm$0.1 ns of the mean value, demonstrating a satisfactory uniformity for the setup. These results are largely independent from the burst search type and parameters. The FRET efficiency estimated from the mean fitted lifetime across the different channels is 0.74. Using the manufacturer reported value R_0 = 6.5 nm for the ATTO550-ATTO647N dye pair, this efficiency corresponds to a theoretical donor-acceptor distance of 5.5 nm. As a comparison, using a simplistic dsDNA model, the donor-acceptor separation of 12 base pairs corresponds to a distance of 4.1 nm. This discrepancy may be due to a different R_0 resulting from local dye environment effects, polarization anisotropy, DNA geometry or dyes linker length effects, which will be examined in future studies.

Next, we consider the mean lifetime obtained from each burst separately. (Fig. 11). For an exponentially distributed random variable, the maximum likelihood estimator of the time-constant is the sample mean. Thus, if a fluorescence decay is mono-exponential and the effects of convolution with the IRF and background are negligible, the lifetime can be estimated by computing the average of all nanotimes. In our case, the donor-only sample is predominantly mono-exponential, and this hypothesis therefore applies. To select a mono-exponential tail on the fluorescence decay, we selected an interval of nanotimes starting where all IRFs decreased to below 1% of their peak value, and ending where the fluorescence decay equal to twice the baseline of the noisiest channel. This criterion resulted in a selection of nanotimes in the 1-18 ns range (identical by definition on all channels) as highlighted in Fig. 9.

Fig. 11 shows the resulting distributions of burst lifetimes. Estimating lifetimes from single bursts results in noisier data. However the center of these distributions are comparable to the lifetimes values estimated by fitting the decays (Fig. 10 A) and are very uniform across the different spots.

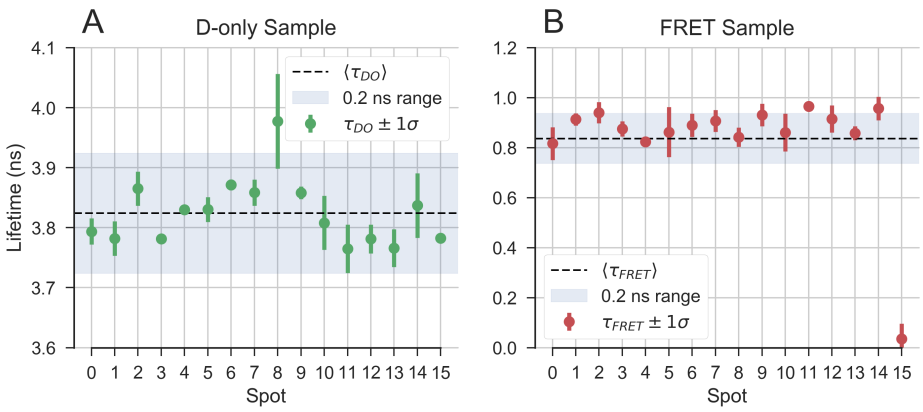

Fig 10 Fitted lifetimes versus channel obtained by fitting the fluorescent decay histograms. For each channel, we performed a non-linear least-squares fitting of two exponential components plus a baseline, convolved with an experimental IRF.

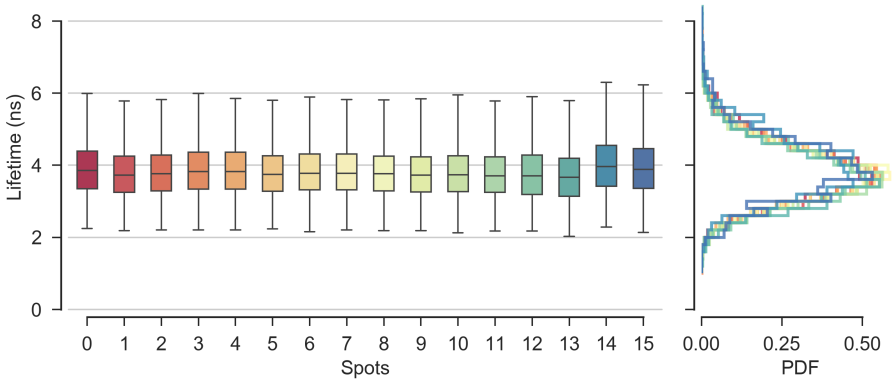

Fig 11 Burst lifetime distributions for the different spots. (*left*) Box-and-whiskers plot of the distribution of burst lifetimes in each spot. The box extends from the lower to upper quartile values of the samples, with a line at the median. The whiskers extend between the 1^{st} and the 99^{th} percentile, thus covering 98% of the data. (*right)* Normalized histograms of burst lifetimes for each of the 16 spots.

4 Conclusions

In this preliminary study, we demonstrated a simple line-excitation scheme combined with new TCSPC SPAD arrays as a compelling approach for high-throughput TCSPC measurement on freely-diffusing single-molecule. We also explored basic performance of the acquisition hardware, which comprises a 16-pixel SPAD array and 16-channel TCSPC module, developed by the Politecnico di Milano group.[14,15] Results show single-molecule detection in all 16 channels and the ability to fit fluorescence decays corresponding to selected populations of single molecule bursts, retrieving lifetime with variations of around 2% across the different channels. The line-excitation approach could be extended to multi-color detection (for smFRET measurement covering the whole FRET range) and multiple laser excitation (i.e. ALEX[6,7] or PIE[8]). The combination of

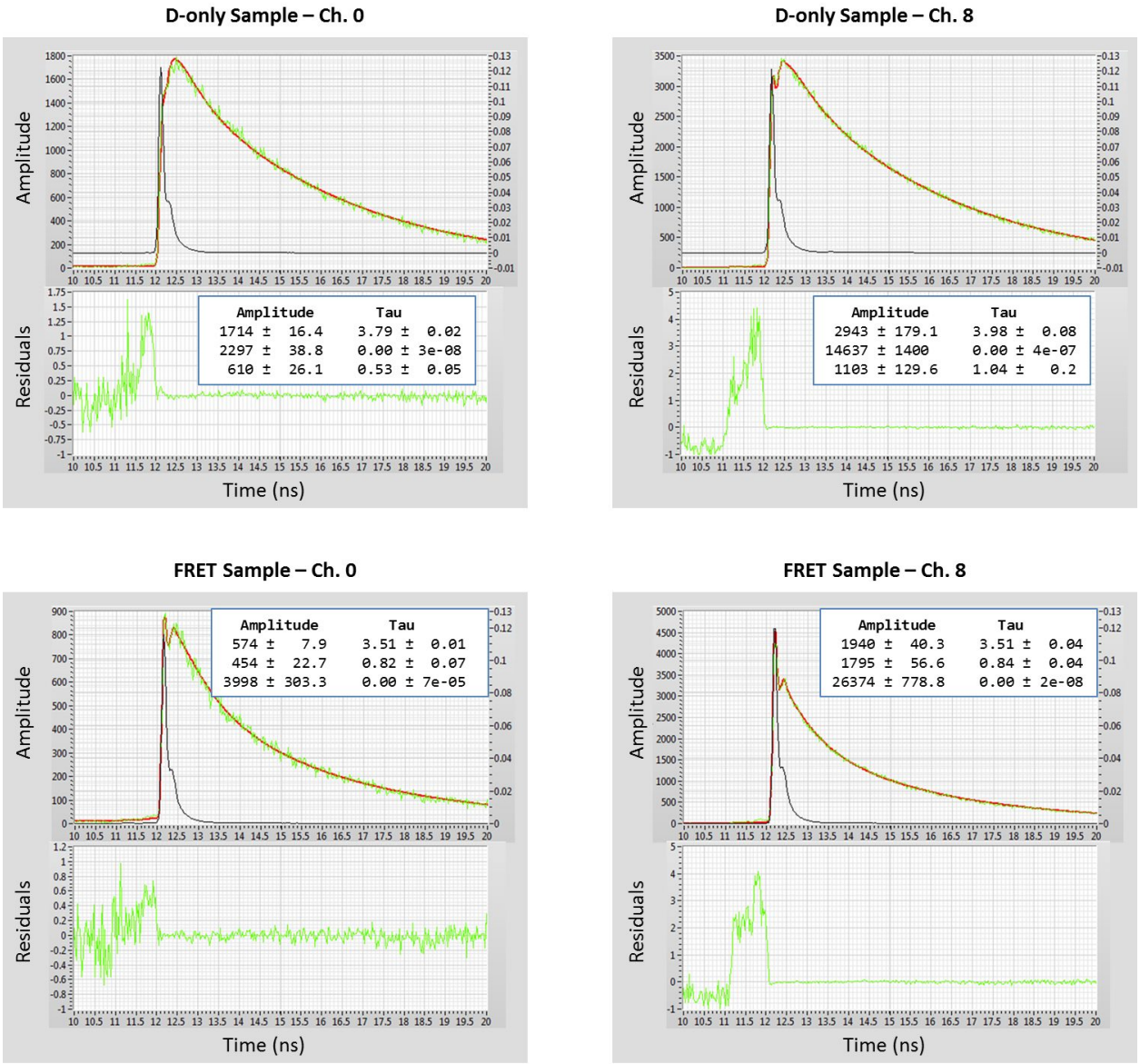

Fig 12 Fluorescence decay histograms fitted to a multi-exponential model. Results are shown for donor-only and FRET samples for two representative channels. The top plot in each of the four panels show the fluorescence decay histogram (*green*), the fitted model (*red*) and the IRF for that channel (*black*). The bottom plot in each panel show the residuals normalized by the decay itself. The model includes three exponential function, a baseline and IRF reconvolution. One of the exponential components is consistently below 10 ps and accounts for scattered background light (Raman or Rayleigh).

this setup with microfluidic devices will open the way to applications such as kinetic studies of biological reactions in freely-diffusing biomolecules in real time,[10] among other possibilities.

Disclosures

S. Weiss discloses equity in Nesher Technologies and intellectual property used in the research reported here. The work at UCLA was conducted in Dr. Weiss's Laboratory. M. Ghioni discloses equity in Micro Photon Devices S.r.l. (MPD). No resources or personnel from MPD were involved in this work.

Acknowledgments

This work was supported by NIH grants R01 GM095904 & R01 GM069709 and NSF grant MCB 1244175.

References

1 S. Weiss, "Fluorescence spectroscopy of single biomolecules.," *Science (New York, N.Y.)* **283**, 1676–1683 (1999). [10.1126/science.283.5408.1676].

2 J. Hohlbein, T. D. Craggs, and T. Cordes, "Alternating-laser excitation: single-molecule FRET and beyond," *Chemical Society Reviews* **43**, 1156–1171 (2014). [10.1039/C3CS60233H].

3 C. Eggeling, J. R. Fries, L. Brand, *et al.*, "Monitoring conformational dynamics of a single molecule by selective fluorescence spectroscopy," *Proceedings of the National Academy of Sciences* **95**, 1556–1561 (1998). [10.1073/pnas.95.4.1556].

4 J. R. Fries, L. Brand, C. Eggeling, *et al.*, "Quantitative Identification of Different Single Molecules by Selective Time-Resolved Confocal Fluorescence Spectroscopy," *The Journal of Physical Chemistry A* **102**, 6601–6613 (1998). [10.1021/jp980965t].

5 C. Eggeling, S. Berger, L. Brand, *et al.*, "Data registration and selective single-molecule analysis using multi-parameter fluorescence detection," *Journal of Biotechnology* **86**, 163–180 (2001). [10.1016/S0168-1656(00)00412-0].

6 A. N. Kapanidis, T. A. Laurence, N. K. Lee, *et al.*, "Alternating-Laser Excitation of Single Molecules," *Accounts of Chemical Research* **38**, 523–533 (2005). [10.1021/ar0401348].

7 T. A. Laurence, X. Kong, M. Jger, *et al.*, "Probing structural heterogeneities and fluctuations of nucleic acids and denatured proteins.," *Proceedings of the National Academy of Sciences of the United States of America* **102**, 17348–17353 (2005). [10.1073/pnas.0508584102].

8 B. K. Müller, E. Zaychikov, C. Bruchle, *et al.*, "Pulsed interleaved excitation.," *Biophysical journal* **89**, 3508–22 (2005). [10.1529/biophysj.105.064766].

9 A. Ingargiola, F. Panzeri, N. Sarkosh, *et al.*, "8-spot smFRET analysis using two 8-pixel SPAD arrays," in *Proceedings of SPIE*, **8590** (2013). [10.1117/12.2003704].

10 A. Ingargiola, E. Lerner, S. Chung, *et al.*, "A Multispot Confocal Platform for High-Throughput Freely Diffusing Single-Molecule FRET Studies," *Biophysical Journal* **110**, 194a–195a (2016). [10.1016/j.bpj.2015.11.1084].

11 X. Michalet, A. Ingargiola, R. A. Colyer, *et al.*, "Silicon Photon-Counting Avalanche Diodes for Single-Molecule Fluorescence Spectroscopy," *IEEE Journal of Selected Topics in Quantum Electronics* **20**, 1–20 (2014). [10.1109/JSTQE.2014.2341568].

12 H. Oikawa, Y. Suzuki, M. Saito, *et al.*, "Microsecond dynamics of an unfolded protein by a line confocal tracking of single molecule fluorescence," *Scientific Reports* **3**, 2151 (2013). [10.1038/srep02151].

13 M. Saito, S. Kamonprasertsuk, S. Suzuki, *et al.*, "Significant Heterogeneity and Slow Dynamics of the Unfolded Ubiquitin Detected by the Line Confocal Method of Single-Molecule Fluorescence Spectroscopy," *The Journal of Physical Chemistry B* **120**, 8818–8829 (2016). [10.1021/acs.jpcb.6b05481].

14 S. Antonioli, L. Miari, A. Cuccato, *et al.*, "8-Channel acquisition system for Time-Correlated Single-Photon Counting.," *The Review of scientific instruments* **84**, 064705–064705 (2013). [10.1063/1.4811377].

15 A. Cuccato, S. Antonioli, M. Crotti, *et al.*, "Complete and Compact 32-Channel System for Time-Correlated Single-Photon Counting Measurements," *IEEE Photonics Journal* **5**, 6801514–6801514 (2013). [10.1109/JPHOT.2013.2284250].

16 W. Becker, *The BH TCSPC Handbook*, Becker & Hickl GmbH, 6th ed. (2015).

17 A. Ingargiola, E. Lerner, S. Chung, *et al.*, "FRETBursts: An Open Source Toolkit for Analysis of Freely-Diffusing Single-Molecule FRET," *PLOS ONE* **11**, e0160716 (2016). [10.1371/journal.pone.0160716].

18 A. Ingargiola, T. Laurence, R. Boutelle, *et al.*, "Photon-HDF5: An Open File Format for Timestamp-Based Single-Molecule Fluorescence Experiments," *Biophysical Journal* **110**, 26–33 (2016). [10.1016/j.bpj.2015.11.013].

19 A. Ingargiola, E. Lerner, and X. Michalet, "16-ch TCSPC single-molecule measurement of dsDNA using line-excitation," (2017). [10.6084/m9.figshare.4625131].

20 J. A. Nelder and R. Mead, "A Simplex Method for Function Minimization," *The Computer Journal* **7**, 308–313 (1965). [10.1093/comjnl/7.4.308].

21 G. R. Phillips and E. M. Eyring, "Error estimation using the sequential simplex method in nonlinear least squares data analysis," *Analytical Chemistry* **60**, 738–741 (1988). [10.1021/ac00159a002].